*LA-UR-04-8109, ASME Journal of Vibration and Acoustics, **128**(4),469-476, 2006*

# Piezoelectric Active Sensor Self-Diagnostics using Electrical Admittance Measurements

Gyuhae Park, Charles R. Farrar, Amanda C. Rutherford, Amy N. Robertson

Engineering Sciences & Applications
The Engineering Institute
Los Alamos National Laboratory
Los Alamos, NM 87545

**ABSTRACT**

This paper presents a piezoelectric sensor self-diagnostic procedure that performs *in-situ* monitoring of the operational status of piezoelectric materials used for sensors and actuators in structural health monitoring (SHM) applications. The sensor/actuator self-diagnostic procedure, where the sensors/actuators are confirmed to be functioning properly during operation, is a critical component to successfully complete the SHM process with large numbers of active sensors typically installed in a structure. The premise of this procedure is to track the changes in the capacitive value of piezoelectric materials resulting from the degradation of the mechanical/electrical properties and its attachment to a host structure, which is manifested in the imaginary part of the measured electrical admittances. This paper concludes with an experimental example to demonstrate the feasibility of the proposed procedure.

## INTRODUCTION

Structural health monitoring (SHM) techniques based on the use of active-sensing piezoelectric materials have received considerable attention in the structural community. The molecular structure of piezoelectric (PZT) materials produces a coupling between electrical and mechanical domains. Therefore, this type of material generates mechanical strain in response to an applied electric field. Conversely, the materials produce electric charges when stressed mechanically. This coupling property allows one to design and deploy an "*active*" and "*local*" sensing system whereby the structure is locally excited by a known input, and the corresponding responses are measured by the same excitation source. Some advantages of these devices are compactness, light-weight, low-power consumption, ease of integration into critical structural areas, ease of activation through electrical signals, higher operating frequency, and low cost. The employment of a known input also facilitates subsequent signal processing of the measured output data.

A critical aspect of the piezoelectric active sensing technologies is that usually large numbers of distributed sensors and actuators are needed to perform the required monitoring process. In addition, the structures in question are usually subjected to various external loading and environmental conditions that may adversely affect the functionality of SHM sensors and actuators. Most current monitoring systems are not intelligent enough to differentiate signal changes caused by damage from those due to sensor failures. The piezoelectric sensor/actuator self-diagnostic procedure, where the sensors/actuators are confirmed to be operational, is therefore a critical component to successfully complete the SHM process. Because piezoceramic materials are brittle, sensor fracture and subsequent degradation of mechanical/electrical properties are the most common types of sensor/actuator failures. In addition, the integrity of

bonding between a PZT sensor and a host structure should be maintained and monitored throughout their service lives.

This paper describes a piezoelectric sensor self-diagnostic procedure based on electrical admittance measurements. The basis of this procedure is to track the changes in the capacitive value of piezoelectric materials, which is manifested in the imaginary part of the measured electrical admittances. Furthermore, through analytical and experimental investigation, it is confirmed that the bonding layer between a PZT sensor and a host structure significantly contributes to the measured electrical admittance. Therefore, by monitoring the imaginary part of the admittances, one can quantitatively assess the fracture or degradation of the mechanical /electrical properties of the PZT sensor and the integrity of its attachment to a host structure. The rest of this paper includes the literature survey, description of the proposed sensor diagnostic method, experimental procedure and results, and several issues that can be used as a guideline for future investigation.

## LITERATURE REVIEW

In general, a completely broken sensor/actuator can be easily identified if a sensor does not produce any measurable output, or an actuator does not reasonably respond to applied signals. However, if only a small fracture occurs within the materials, the sensors/actuators are still able to produce sufficient performance (with distorted signals after the sensor fracture), potentially leading to a false indication of the structural condition. For piezoelectric sensors, sensor failures are inevitable after extreme natural hazards, such as an earthquake, because sensors are usually the most delicate part in structural systems. Furthermore, the mechanical and electrical properties of PZT materials can gradually degrade over their service lives. This degradation of

sensor quality, as well as degradation in bonding integrity, will be especially problematic, if one needs to employ large numbers of sensors/actuators over a long period time and to identify when to replace the sensor/actuator network. To the authors' best knowledge, however, the issues associated with long-term reliability of the PZT sensors under the real-world operational condition, and the methods and metrics that can be used to assess the degradation of the piezoelectric sensor/actuator quality have not been sufficiently addressed in the literature.

The importance of bond integrity between a PZT wafer and a host structure can be understood intuitively. The fundamental assumption in piezoelectric active-sensing technologies is that the sensors and actuators are perfectly bonded to a structure, and the integrity of the bonding layer does not change throughout their service lives, which is not the case in real-world applications. For instance, the adhesives used for bonding the PZT patch have a finite service life, usually shorter than the host structure's life-span.

Contrary to the breakage or the degradation of the sensor quality, a great amount of research efforts have been focused on understanding the effects of the bonding layer on the sensor/actuator performance [1-11]. Through experimental and analytical investigation, these studies showed that the effects of bonding defects are remarkable, modifying stress and strain transfer mechanisms [2,4,5,8], frequency spectrums including modal frequencies and damping ratio [1,3], performance of closed-loop vibration controls [3,6], performance of constrained layer damping [9], and measured electrical impedances[7,10].

Crawley and De Luis [12], Park et al. [13] and Sirohi and Chopra [14]have demonstrated the effects of the bond layer on the induced strain transfer mechanisms for surface bonded PZT wafers, referred to as shear lag effect. The shear lag ratio, $\xi=(S_p/S_b - 1)$, where $S_p$ and $S_b$ are the PZTs' and the structure's strain, respectively, is defined as in the following equation. In perfect bonding ($S_p=S_b$), the shear lag ratio is equal or close to zero.

$$\frac{\partial^2 \xi}{\partial x^2} - \Gamma^2 \xi = 0 \tag{1}$$

and

$$\Gamma^2 = \left( \frac{G_s}{Y_p t_s t_c} + \frac{3 G_s w}{Y_b w_b t_b t_c} \right) \tag{2}$$

where $x$ is the longitudinal direction of a beam, $G_s$ is the shear modulus of bonding material, $Y_p$ and $Y_b$ are the Young's moduli of the PZT material and the structure, respectively, $t_s$, $t_c$ and $t_b$ are the thicknesses of the bonding layer, PZT material and the structure, respectively, and $w$ and $w_b$ are the widths of the PZT material and the structure, respectively. $\Gamma$ is defined as the shear lag parameter. This equation and further analysis indicate that, if the PZT wafer is used as a sensor, the sensing voltage generated by the host structure's strain is less than that of a perfectly bonded condition, and hence underestimates the strain in the substructure. From the above equations, one can clearly infer that the shear lag effect, which modifies the PZT sensing mechanisms, is a function of the geometry and mechanical properties of the PZT material ($t_c$, $w$, $Y_p$) and those of the bonding materials ($t_s$, $G_s$). In order to reduce the shear lag phenomenon, one needs to use higher shear modules adhesives and keep the thickness of the bonding layer as thin as possible, as indicated by Eq. (2). Changes in these properties can be considered as the degradation of the bonding quality.

While there are many studies in the literature identifying the performance of a PZT patch with a known debonding issue, a literature search shows that there are only a few studies investigating how to assess the quality of the bonding condition. Saint-Pierre et al [15] proposed a new debonding identification algorithm by monitoring the resonance of a PZT sensor measured by electrical impedances. As the de-bonding area between the PZT wafer and the host increases, the shape of the PZT wafer's resonance becomes sharper and more distinctive, and the magnitudes of the host resonances are reduced. Essentially the same approach was proposed by Giurgiutiu et al [16]. However, because of the mechanical impedance mismatching between the PZT patch and the host, the method is not sensitive to small debonds. In addition, this method is not able to account for the sensor fracture that may simultaneously occur with the debonding process, because the sensor breakage would apparently change the resonances of a PZT sensor. Sun and Tong [17] proposed a closed loop-based debonding identification scheme. The premise of the method is to use a sensitive control system that can be destabilized by a slight frequency shift caused by small edge debonding in a PZT patch. Although the method shows great sensitivity, only 0.1% of debonding in a simulation study, the issues associated with how to differentiate the frequency shift caused by structural damage from that of actuator debonding was not fully addressed.

It is apparent that the importances of sensor self-diagnostic procedures that address the conditions of both sensors and the bond have received little attention in literature. In order to fully implement current active-sensing systems in practice beyond proof-of-concept demonstration, the authors believe that an efficient sensor-self diagnostic procedure should be adopted in the SHM process, forming the motivation of this study.

## SENSOR SELF-DIAGNOSTICS USING ADMITTANCE MEASUREMENTS

The premise of the proposed sensor self-diagnostic procedure is to track the changes in the imaginary part of the electrical admittance of the piezoelectric materials. In this section, we theoretically and experimentally demonstrate that the degradation of the mechanical/electrical properties of the PZT sensors and its attachment to the external structure produces measurable and distinct changes in the PZT's measured admittances.

Piezoelectric transducers acting in the direct manner produce an electrical charge when stressed mechanically. Conversely, a mechanical strain is produced when an electrical field is applied. The effects of piezoelectricity between the electrical and mechanical variables can be described by the following linear relations [18],

$$S_i = s_{ij}^E T_j + d_{mi} E_m \tag{3}$$

$$D_m = d_{mi} T_i + \varepsilon_{mk}^T E_k \tag{4}$$

where $S$ is the mechanical strain, $T$ is the mechanical stress, $E$ is the electric field, $D$ is the charge density, $s$ is the mechanical compliance, $d$ is the piezoelectric coupling constant, $\varepsilon$ is the dielectric constant of the PZT material, and the subscripts $i$, $j$, $m$ and $k$ indicate the direction of stress, strain or electric field. The superscripts $E$ and $T$ indicate that those quantities are measured at zero electric field and zero stress, respectively. The first equation describes the converse piezoelectric effect and the second one describes the direct piezoelectric effect.

Differentiating the charge density with respect to time and integrating it over the effective electrode area yields the total electric current flowing through the PZT wafer. For an one-

dimensional case, the electric current ($I$) of the free piezoelectric transducer is calculated from Eq. (4), when $T = 0$,

$$\begin{aligned} I &= i\omega \iint D_3 dxdy \\ &= i\omega \iint \varepsilon_{33}^{\ T}(1-\delta) E_3 dxdy \end{aligned} \tag{5}$$

where $\omega$ is the angular frequency, $\delta$ is the dielectric loss tangent of the PZT material, and $x$, $y$ are the plane coordinates of a PZT patch. The subscript 3 indicate the charge density is along the $z$-axis perpendicular to the $x$-$y$ (1-2) plane. Note that a uniform distribution of the charge density within the PZT material is assumed in the integration. Then, the electrical admittance of a free PZT transducer, which is defined as the ratio of the energizing voltage to the resulting current, is given in the following relation.

$$Y_{free}(\omega) = \frac{I}{V} = i\omega \frac{wl}{t_c}\left(\varepsilon_{33}^{\ T}(1-i\delta)\right) \tag{6}$$

where $V$ is the applied voltage, and $w$, $l$, $t_c$ is the width, length and thickness of a PZT patch, respectively.

When a PZT patch is surface-bonded to a structure, Liang et al. [19] shows that the electrical admittance $Y(\omega)$ of the PZT transducer is a combined function of the mechanical impedance of the host structure $Z_s(\omega)$ and that of the PZT transducer $Z_a(\omega)$, in addition to the terms in Eq. (6), given by;

$$Y(\omega) = i\omega \frac{wl}{t_c}\left(\varepsilon_{33}^{\ T}(1-i\delta) - d_{31}^{\ 2} Y_p^E + \frac{Z_a(\omega)}{Z_a(\omega)+Z_s(\omega)} d_{31}^{\ 2} \hat{Y}^E \left(\frac{\tan kl}{kl}\right)\right) \tag{7}$$

where $Y_p^E$ is the complex Young's modulus of the PZT material at zero electric field. The wave number of the PZT patch, *k*, is given by,

$$k = \omega \sqrt{\frac{\rho}{\hat{Y}^E}} \tag{8}$$

where $\rho$ is the mass density of the PZT material. Equation (7) is derived based on an assumption that a PZT patch is attached to one end of a structural system, whereas the other end of the PZT patch is fixed. This assumption regarding the interaction at two discrete points is consistent with the mechanism of force transfer from the bonded PZT transducer to the structure.

Equation (7) sets groundwork for using the PZT sensors/actuators for impedance-based structural health monitoring applications. Assuming that the mechanical and electrical property of the PZT wafer does not change over the monitoring period of the host structure, Equation (7) clearly shows that the electrical admittance or impedance of the PZT material is directly related to the mechanical impedance of the host structure, allowing for the monitoring of the host structure's mechanical properties using the measured electrical property. A complete description of the electro–mechanically coupling impedance modeling principle, which is discussed by Equation (3)-(7), and its application to structural health monitoring can be found in the reference [10, 20, 21]

The proposed sensor diagnostic process is based on Eqs. (6) and (7). The admittance of a PZT material is clearly a function of its geometry constants (*w, l,* $t_c$), mechanical properties ($Y_p^E$), and electrical properties ($\varepsilon_{33}^T$, $d_{31}$, $\delta$). It is also obvious from the equations that the changes in these properties are manifested more distinctly in the imaginary part of the electrical admittance.

Therefore, the breakage of the sensor and the degradation of the sensor's quality can be identified by monitoring the imaginary part of the electrical admittance. These changes would cause a downward shift in the slope.

Another significant observation that can be made from Eqs. (6) and (7) is that one can identify the effect of the bonding layer on the measured electrical admittance. The effect of the bonding layer is obtained by letting $Z_s(\omega)$ be $\infty$ in Eq. (7),

$$Y_b(\omega) = i\omega \frac{wl}{t_c}\left(\varepsilon_{33}^{T}(1-i\delta) - d_{31}^{2}Y_p^E\right) \tag{9}$$

It is clear from Eqs. (6) and (9) that the electrical admittance of the same PZT material would be different if under a free-free condition or surface-bonded (or commonly referred to as blocked) condition. The blocked condition would cause a downward shift in the slope of the electrical admittance of a free PZT patch with the factor of $d_{31}^{2}Y_p^E$. The assumption that $Z_s(\omega) = \infty$ would be valid, especially at a lower frequency range, because the mechanical impedance of the structure in question is usually several orders of magnitude greater than that of a PZT transducer. In other words, the piezoelectric active sensors used for structural health monitoring (usually) have much smaller mass and stiffness compared to those of a host structure being monitored at relatively lower frequency ranges. Even though this derivation does not explicitly consider the parameters of bonding materials such as thickness or shear modulus, it is obvious from Eq. (9) that the use of a PZT transducer with lower $Y_p^E$ will reduce the effect of the bond on the measured admittance, which is consistent with the shear lag loss, shown in Eq. (2).

Figure 1 shows the measured admittance of free and surface bonded PZT patches. The 5A PZT materials with dimensions of 20 x 20 x 0.25 mm are used. The admittances of three free PZT patches were measured in the frequency range of 40-20,000 Hz using an Agilent 4294A impedance analyzer. These PZT patches were then surface-mounted to a thick aluminum beam and plate using an epoxy with vacuum bagging to ensure a better bonding condition. The admittance measurements were then repeated.

As can be seen in Figure 1, the downward shifting effect of the bonding layer is remarkable. The slope of the imaginary part, which is analogous to the capacitive value of the PZT material, was changed from 2.91e-7 to 1.8e-7, resulting in a 38 % reduction. Analytically, however, it has been estimated as a 22 % downward shift. It is believed that this discrepancy is coming from the shear modulus of the bonding materials, which is not included in the analysis of Eq. (9). The shear modulus of the thin bonding layer may increase the effective Young's modulus of the PZT patch in Eq. (9). In addition, the bonding layer also contains capacitive dielectric constants connected directly to the PZT patch in series, resulting in the downward shift of the measured admittance. Therefore, Equation (9) can only be used to qualitatively assess the effect of the bonding layer. A more improved modeling technique, which incorporates the comprehensive electromechanical effects of the bonding layer, would be required for more quantitative estimation of the effect on the measured electrical admittance and is currently being investigated by authors.

Nevertheless, the importance of this analysis is that the bonding layer contributes to the overall admittance of PZT patches bonded to a structure. Thus, bonding defects would also affect the

measured admittance. Contrary to the sensor breakage, bonding defects would cause an upward shift in the slope of the imaginary part of the electrical admittance. Therefore, the sensor functionality including the sensor breakage and the degradation of the bonding condition can be assessed by monitoring the imaginary part of the admittances.

It should be noted that, for surface-bonded PZT patches, the resonance of the structures are clearly observed in their responses, as shown in Figure 1. This resonant response confirms that the electrical admittance or impedance of surface-bonded piezoelectric patches represents the unique dynamic characteristics of the host structure, which is the basis of the impedance-based health monitoring technique [10, 20, 21]. It is important to point out that the changes associated with the sensor functionality are, however, clearly discernible from those of structural damage. Because of the capacitive nature of PZT materials, the real part of the admittance/impedance has been mainly used for monitoring in applications [21]. The changes resulting from the structural damage will cause complete changes in real part of the admittance/impedance signatures, while causing variations along the imaginary part of the signatures (no change in the slope). On the other hand, sensor failure will result in changes to both the real and imaginary part of the admittance/impedance signatures, causing a downward (sensor breakage) and an upward (debonding between PZT transducers and the host) shift in the slope of the imaginary part of the admittance.

To use the proposed sensor diagnostic procedure, one needs measured electrical admittance response data from a PZT wafer, which can be easily accomplished by using a simple impedance/admittance measuring circuit [22]. A data acquisition system with higher sampling

frequencies is not necessary because this method is more efficient at lower frequency ranges, up to only several kHz. At higher frequencies, the assumption of $Z_s(\omega) = \infty$ is no longer valid, because the mechanical impedance of the PZT patch becomes comparable to that of the structure as the structural response is getting dominated by local modes (not global modes). This characteristic will significantly relax the hardware requirement for the proposed sensor diagnostic procedure. Furthermore, just one such device would be required to check large numbers of sensors and actuators placed in a structure. This proposed method will be very effective in providing a metric that can be used to determine the sensor functionality over a long period of time or after an extreme loading on a structure. The proposed sensor diagnostic procedure can be also useful if one needs to check the operational status of a sensing network right after its installation.

## EXPERIMENTAL INVESTIGATION

An experiment was performed to check the validity of the proposed concept. Rather than quantitatively assessing the degree of sensor failures, the objective of this experiment was to determine if the sensors are operating correctly using the proposed sensor diagnostic procedure, for those that are surface-mounted on a structure subjected to extensive impact loadings. This procedure is taken because the control of slight sensor breakages or bonding defects is difficult to obtain experimentally. Controlled projectile impact experiments using a gas gun were conducted on a graphite/epoxy-fiber-reinforced composite plate with surface-bonded PZT transducers. These impacts could be considered as one of operational condition in real-world applications, such as used in unmanned aerial vehicles [23].

***Experimental Setup***

The test structure is shown in Figure 2. The dimension of the quasi-isotropic composite plate is 609 x 609 x 6.35 mm. The lay-up contains 48 plies stacked according to the sequence [6(0/45/-45/90)]s using 60% Toray T300 graphite fibers in a 934 Epoxy matrix. Two pairs of piezoelectric (5A) and Macro-Fiber Composite (MFC) patches are mounted on one surface of the plate, as shown in Figure 2. The sizes of the PZT patch and MFC are 25.4 x 25.4 x 0.254 mm and 25.4 x 12.7 x 0.254 mm, respectively. The MFC are a relatively new type of piezoelectric sensors that are more flexible than the conventional PZT materials [24, 25]. The Young's Modulus of a flexible MFC is 15 GPa, only a fifth of traditional piezoceramic materials (5A, 66 GPa). As described earlier, the MFCs are expected to be less affected by the shear lag loss or bonding defects than traditional PZT patches because of the lower value in $Y_p^E$.

In order to measure the electrical admittance of the PZT patch, a simple impedance measuring circuit was used [22]. The electrical admittance is defined as the ratio between the applied voltage and the resulting current, as shown in Eq. 10. Hence, the input voltage into the PZT patch and the output voltage from the PZT circuit, which is proportional to the resulting current within the materials as seen in Figure 3, are used to estimate the admittance. Electrical admittance of the PZT patch is obtained through the following equation:

$$Y_p = \frac{I}{V} = \frac{V_{out}/R}{V_{in} - V_{out}} \tag{10}$$

A commercial data acquisition system controlled from a laptop PC is used to digitize the voltage analog signals at a sampling rate of 51.2 kHz, producing 32,768 time domain data points. An

amplified random signal (1 V) is used as the voltage input for the testing. All time history data are first standardized by subtracting the mean and dividing by the standard deviation, as in the Eq. (11).

$$\overline{\mathbf{x}} = \frac{\mathbf{x} - \mu}{\sigma} \tag{11}$$

where $\mathbf{x}$ is the original vector, $\overline{\mathbf{x}}$ is the normalized vector, $\mu$ is the mean of the original vector, and $\sigma$ is the standard deviation of the original vector. This process was previously used to reduce the environmental and operational variability [26]. This process eliminates DC bias and normalizes the variations associated with the differences in excitation levels, which can be caused by changes in the damping of a host structure with respect to temperature variations. Each time history is split up into 29 separate 4096-point blocks, with 75% overlap. A Fast Fourier Transform is then performed on all data blocks in order to transfer the time history information into the frequency domain for the admittance estimate.

A total of 14 baseline measurements with the PZT patches and MFCs were recorded to capture environmental variability before the impacts were introduced. The baselines were measured under different ambient and temperature conditions over a three week period. Before the first impact test, two cables were attached to two sides of the plate so that that plate could hang from the test frame in a nearly free-free condition. Impact loading was then introduced to the plate by firing a small projectile out of a gas gun. A gas gun is used to propel a 192.3g steel projectile with a spherical nose at the composite plate. Five shots aimed at different locations and at varied velocities (31.09 m/s, 39.93 m/s, 36.88 m/s, 35.66 m/s, 32.92 m/s) created different damage scenarios. The impact locations are shown in relation to the PZT and MFC sensors in Figure 4,

and summarized in Table 1. No physically visible structural damage was identified during the tests except for Impact 2. Impact 2, with the highest velocity, caused visible damage to the plate. Other impacts, including Impacts 3, 4, and 5, introduced subsurface delamination to the plate, which was identified using an ultrasonic C-scan method. The admittance measurements were repeated after each impact to asses the condition of the PZT and MFC sensors.

***Experimental Results***

Fourteen admittance baseline measurements obtained from PZT 1 and PZT 2 are shown in Figure 5 in the frequency range 0-20 kHz. The temperature variations during the three week test period are estimated to be in the range of $\pm 7\ ^{o}C$. Several other boundary condition changes are also manually imposed including horizontal and vertical positioning of the plate, suspending the plate with cables to simulate a free-free condition, or resting on soft forms or hard blocks. As can be seen in the figure, the admittance measurements are quite repeatable. The slope of the admittance remains essentially the same over the three week test period, which shows that the admittance measurements are not affected by different structural conditions. The slopes of the admittance measured from PZT 1 and PZT 2 are also the same, confirming that the bonding conditions for both PZT sensors are approximately identical.

Figure 6 shows the admittance measurement from PZT 1 after induced impacts. When Impact 1 (31.09 m/s) was induced, no change in the response was observed, as shown in the first plot in Figure 6, indicating that no degradation of sensor functionality was introduced by Impact 1. Impact 2 (39.93 m/s) produced considerable changes in response, causing a 20% downward shift in the slope, which may indicate that an internal fracture occurred within the sensor. Using an

ultrasonic C-scan method, the structural delamination induced by Impact 2 was identified, as shown in Figure 7. The increasingly dark region shows delamination between different plys, with the darkest area near the surface of the impact zone. This structural delamination was located partially under the PZT 1, and it is believed that this ply delamination caused a partial sensor breakage of PZT 1. The measurement taken after Impact 3 did not show any noticeable changes and followed the same pattern as that of Impact 2. After Impact 4, an upward shift of the admittance slope was observed compared to previous readings. This could be considered as an indication of debonding. After several impacts, the integrity of the bonding condition is compromised and the result is an upward shift of the admittance slope. After Impact 5, it has been visually observed that PZT 1 was broken, as shown in Figure 8.

The impacts also induced failure in PZT 2, as shown in Figure 9. Impact 1 did not cause any changes, as in the case of PZT 1. A slight upward shift after Impact 2 was identified, which indicates the degradation in the bonding condition. Impact 2, with the highest velocity, obviously caused the sensor fracture of PZT 1 and the debonding defect in PZT 2. Impact 3, which is the closet to the PZT 2, in turn, caused sensor breakage, shifting the admittance slope downward. Impact 4 shows slight change, and Impact 5 shows anther an upward shift of the slope, confirming that the bonding condition is continuously deteriorating.

As shown in this section, the imaginary part of the admittance signature provides a unique feature that can be used for sensor diagnostics procedure. The condition of sensor functionality, including sensor breakage and bonding defects, can be assessed by monitoring this feature. It is important to point out that, even with the degraded conditions, the piezoelectric patches were still

able to produce sufficient sensing and actuation capabilities. The measured responses are significantly distorted partially by the induced delamination on the structure, but the majority of these changes are believed to come from the sensor failure. This type of sensor failure should be identified before the SHM data processing, if one wants to avoid a false indication regarding the structural health.

On the other hand, MFC sensors provide a superior capability compared to the PZT material. Neither of the two MFC sensor's integrity was compromised with the induced impacts. The admittance signatures did not show any noticeable changes. The admittance measurements before and after the impacts are almost identical, as shown in Figure 10. This flexible sensor certainly provides the advantage of being robust and reliable compared to other available piezoceramic sensors. The MFC sensors are confirmed to be continuously functioning after the impacts and hence, be allowed to monitor the conditions of the structure. The SHM results using these MFC sensors can be found in the reference [27].

## DISCUSSION

A piezoelectric active sensor self-diagnostic procedure based on the admittance measurements is proposed. While this procedure can efficiently monitor the condition of the sensor functionality, there are still several research issues remaining for further investigation.

It is envisioned that the proposed sensor diagnostic technique (for bonding condition monitoring) is inefficient for the PZT active sensors installed to extremely thin or tiny structures, as in this case the assumption $Z_s(\omega) = \infty$ is no longer valid. Furthermore, the proposed technique cannot

be used to check the installation status of piezoelectric stack actuators as the mechanical impedance of the actuator is comparable to that of the structures at all frequency ranges. For these cases, the proposed procedure should only be used to check the sensor fractures and the degradation of the mechanical or electrical property of the active sensors.

It is believed that, although the relationship between the sensor breakage and the degree of the downward shift in the admittance slope is quite linear, the bonding defects may not show up in the linear relation in the admittance measurement. An improved modeling that incorporates the effects of the bonding layer on the electrical admittance is required for more quantitative estimation of the bonding defects. This analytical model will also help to identify the sensitivity of the proposed procedure. A more controlled experiment that is able to regulate the degree of sensor failure is required to validate such modeling efforts.

The capacitance of piezoelectric materials is known to be temperature sensitive. A recent study shows that every 5.5 °C change in temperature results in a one percent change in capacitance of the PZT material [28]. Feature identifications and signal processing techniques that are able to normalize the measured admittance data with respect to varying environmental conditions are essential if one is to fully apply the proposed sensor diagnostic process. The development of an automated data-processing algorithm to easily interpret the measured admittance signals, coupled with a stand-alone admittance measuring device, is also required to implement the proposed concept to field applications. These issues are currently being investigated by authors and are the subjects of the next paper.

## CONCLUSION

A piezoelectric sensor self-diagnostic procedure that performs in-situ monitoring of the operational status of piezoelectric sensors and actuators was presented. The basis of this procedure is to track the changes in the measured admittance of piezoelectric materials. Both degradation of the mechanical/electrical properties of a PZT patch and bonding defects between a PZT transducer and a host structure could be identified using the proposed procedure. The feasibility of the method was demonstrated by impact testing on a composite plate, where the functionality of surface-mounted piezoelectric sensors was continuously deteriorated. The proposed sensor diagnostic procedure can provide a metric that can be used to determine the sensor functionality over a long period of service time or after an extreme loading event.

## ACKNOWLEDGEMENT

This research was funded through the Laboratory Directed Research and Development program, entitled “Damage Prognosis Solution,” at Los Alamos National Laboratory.

## REFERENCE

[1] Seeley, C.E., Chattopadhyay, A., 1998. “Experimental Investigation of Composite Beams with Piezoelectric Actuation and Debonding,” *Smart Materials and Structures*, **7**, pp. 502-511.

[2] Wang, X.D., Meguid, S.A., 2000. “On the Electroelastic Behaviors of a Thin Piezoelectric Actuator Attached to an Infinite Host Structures,” *International Journal of Solids and Structures*, **37**, 3231-3251.

[3] Sun, D., Tong, L., Atluri, S.N., 2001. "Effects of Piezoelectric Sensor/Actuator Debonding on Vibration Control of Smart Beams," *International Journal of Solids and Structures*, **38**, pp. 9033-9051.

[4] Tong, L., Sun, D., Atluri, S.N., 2001. "Sensing and Actuation Behaviors of Piezoelectric Layers with Debonding in Smart Beams," *Smart Materials and Structures*, **10**, pp. 713-723.

[5] Rabinovitch, O., Vinson, J.R., 2002. "Adhesive Layer Effects in Surface-mounted Piezoelectric Actuators," *Journal of Intelligent Material Systems and Structures*, **13**, pp. 689-704.

[6] Sun, D.C., Tong, L., 2002. "Control stability analysis of smart beams with debonded piezoelectric actuator layer," *AIAA Journal*, **40**, pp. 1852–1858.

[7] Xu, Y.G., Liu, G.R., 2002. "A Modified Electro-mechanical Impedance Model of Piezoelectric Actuator-sensors for Debonding Detection of Composite Patches," *Journal of Intelligent Material Systems and Structures*, **13**, pp. 389-396.

[8] Faria, A.R., 2003. "The impact of finite-stiffness Bonding on the Sensing Effectiveness o Piezoelectric Patches," *Smart Materials and Structures*, **12**, pp. 5-8.

[9] Sun, D., Tong, L., 2003. "Effect of Debonding in active constrained layer damping patches on hybrid control of smart beams," *International Journal of Solids and Structures*, **40**, pp. 1633-1651.

[10] Bhalla, S., Soh, C.K. 2004. "Electro-Mechanical Impedance Modeling for Adhesively Bonded Piezo-Transducers," *Journal of Intelligent Material Systems and Structures*, **15**, pp.955-972.

[11] Wu, T., Ro, P.I., 2004. "Dynamic Peak Ampitude Analysis and bonding Layer Effects of Piezoelectric Bimorph Cantilevers," *Smart Materials and Structures*, **13**, 203-210.

[12] Crawley, E. F., de Luis, J., 1987. "Use of Piezoelectric Actuators as Elements of Intelligent Structures," *AIAA Journal,* **25**, pp. 1373–1385.

[13] Park, C., Walz, C., Chopra, I., 1996. "Bending and Torsion Models of Beams with Induced-Strain Actuators," *Smart Materials and Structures*, **5**, pp. 98-113.

[14] Sirohi, J., Chopra, I., 2000. "Fundamental Understanding of Piezoelectric Strain Sensors," *Journal of Intelligent Material Systems and Structures*, **11**, pp. 246-257.

[15] Saint-Pierre, N., Jayet, Y., Perrissin-Fabert, I., Baboux, J.C., 1996. "The Influence of Bonding Defects on the Electric Impedance of Piezoelectric Embedded Element," *Journal of Physics D (Applied Physics)*, **29**, pp. 2976-2982.

[16] Giurgiutiu, V., Zagarai, A. Bao, J.J., 2002. "Piezoelectric Wafer Embedded Active Sensors for Aging Aircraft Structural Health Monitoring," *International Journal of Structural Health Monitoring*, **1**, pp. 41-61.

[17] Sun, D., Tong, L., 2003. "Closed-loop Based Detection of Debonding of Piezoelectric Actuator Patches in Controlled Beams," **40**, pp. 2449-2471.

[18] Crawley, E.F., Anderson, E.H., 1990. "Detailed Models of Piezoceramic Actuation of Beams," *Journal of Intelligent Material Systems and Structures*, **1**, pp. 4-25.

[19] Liang, C., Sun, F.P., and Rogers, C.A., 1994. "Coupled Electromechanical Analysis of Adaptive Material System – Determination of Actuator Power Consumption and System Energy Transfer," *Journal of Intelligent Material Systems and Structures,* **5**, pp. 21-20.

[20] Giurgiutiu, V. Zagrai, A.N., 2002. "Embedded Self-Sensing Piezoelectric Active Sensors for Online Structural Identification," ASME *Journal of Vibration and Acoustics*, **124**, pp. 116-125

[21] Park, G., Sohn, H., Farrar, C.R., Inman, D.J., 2003. "Overview of Piezoelectric Impedance-based Health Monitoring and Path Forward," *The Shock and Vibration Digest,* **35**, pp. 451-463.

[22] Peairs, D., Park, G., Inman, D.J., 2004. "Improving Accessibility of the Impedance-based Structural Health Monitoring Method," *Journal of Intelligent Material Systems and Structures*, **15**, pp. 129-140.

[23] Farrar, C.R., Hemez, F.M., Park, G., Robertson, A., Sohn, H., Williams, T., 2004, "Developing Impact and Fatigue Damage Prognosis Solutions for Composites," *JOM-Journal of Minerals, Metals & Materials Society*, **56**, pp. 40-42.

[24] Wilkie, W.K., Bryant, R.G., High, J.W., Fox, R.L., Hellbaum, R.F., Jalink, A., Little, B.D., Mirick, P.H., "Low-cost piezocomposite actuator for structural control applications," *Proceedings of the 7th SPIE International Symposium on Smart Structures and Materials*, Newport Beach, CA, March 5-9, 2000, SPIE publishing

[25] Sodano, H.A., Park, G., Inman, D.J., 2004, "An Investigation into the Performance of Macro-Fiber composites for Sensing and Structural Vibration Applications," *Mechanical Systems and Signal Processing*, Vol. 18, No. 3 pp. 683-697.

[26] Sohn, H., Farrar, C.R., 2001. "Damage Diagnosis using Time Series Analysis of Vibration Signals," Smart Materials and Structures, **10**, pp. 446-451

[27] Park, G., Rutherford, C.A., Wait, J.R., Nadler, B.R, Farrar, C.R., 2004, "The Use of High Frequency Response Functions for Composite Plate Monitoring with Ultrasonic Validation," *AIAA Journal*, **43,** pp.2431-2437.

[28] Simmers, G.E., Hodgkins, J., Mascarenas, D., Park, G., Sohn, H., 2004. "Improved Piezoelectric Self-sensing Actuation," *Journal of Intelligent Material Systems and Structures*, **15**, pp. 941-953.

## LIST OF FIGURES



## LIST OF TABLES

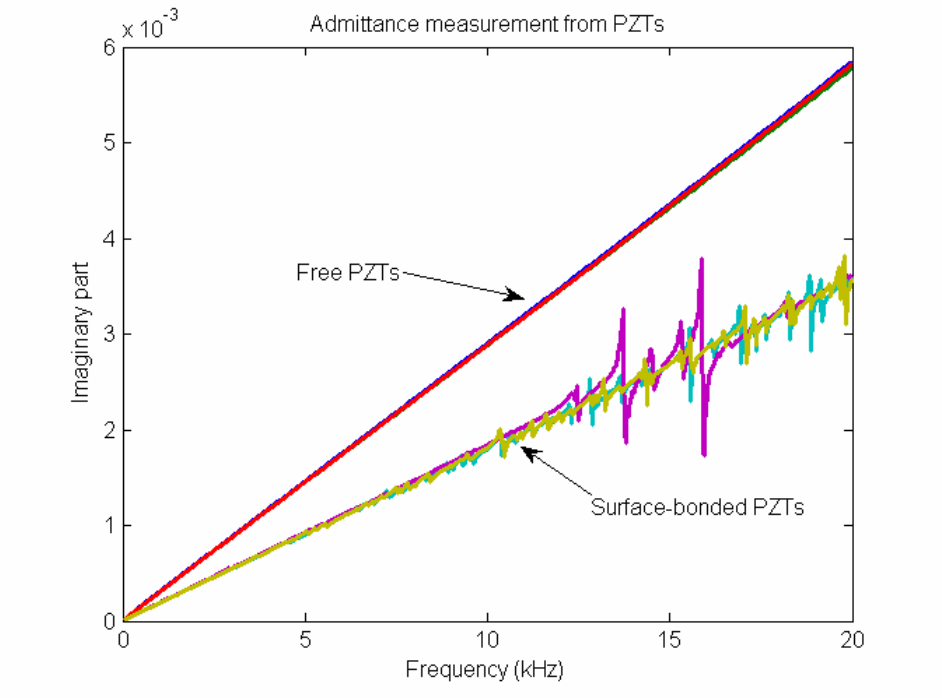


**Figure 1:** Electrical Admittance Measurement from PZT patches under free and surface-bonded conditions

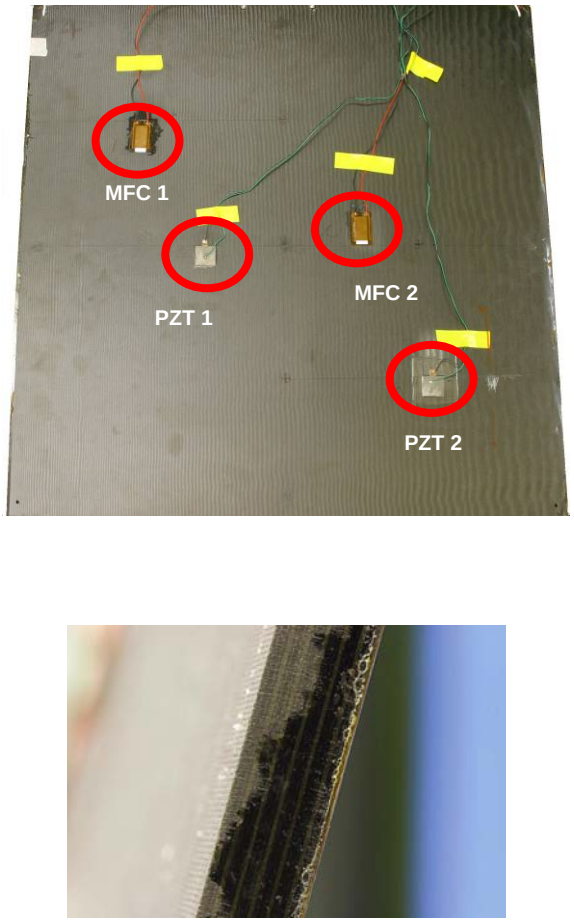


**Figure 2:** The composite plate used for the test.

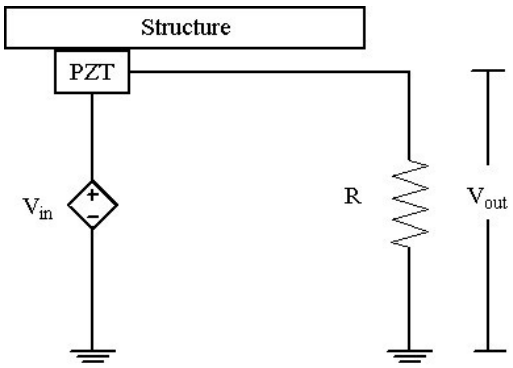


**Figure 3:** Diagram of PZT circuit indicating locations of measured voltages $V_{in}$ and $V_{out}$

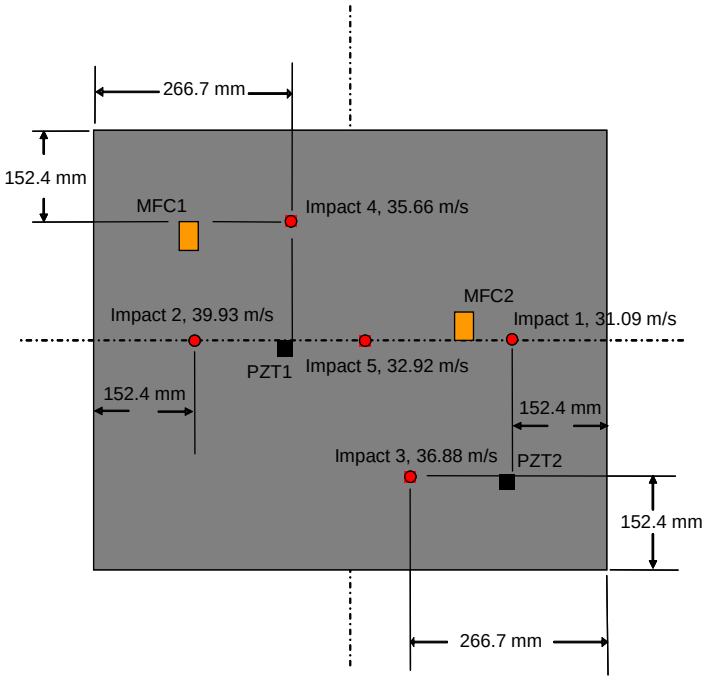


**Figure 4:** Locations of MFC/PZT sensors and the impact

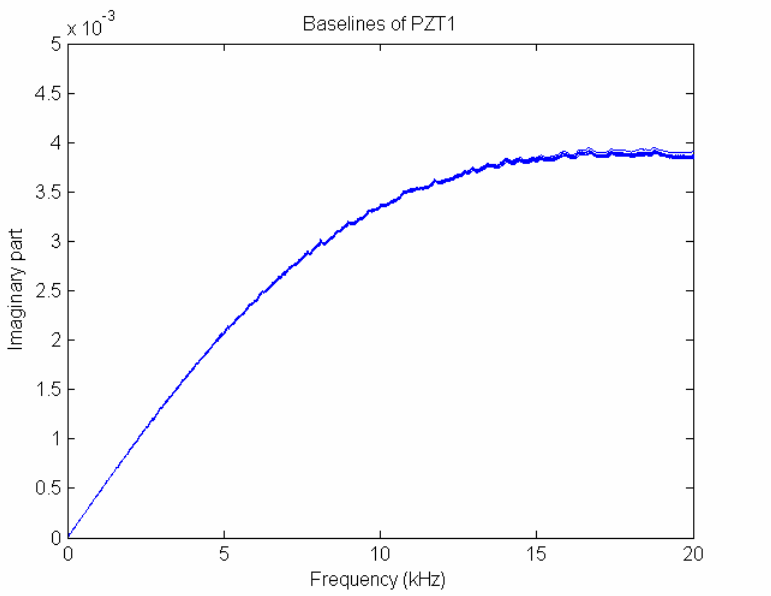


(a) PZT 1

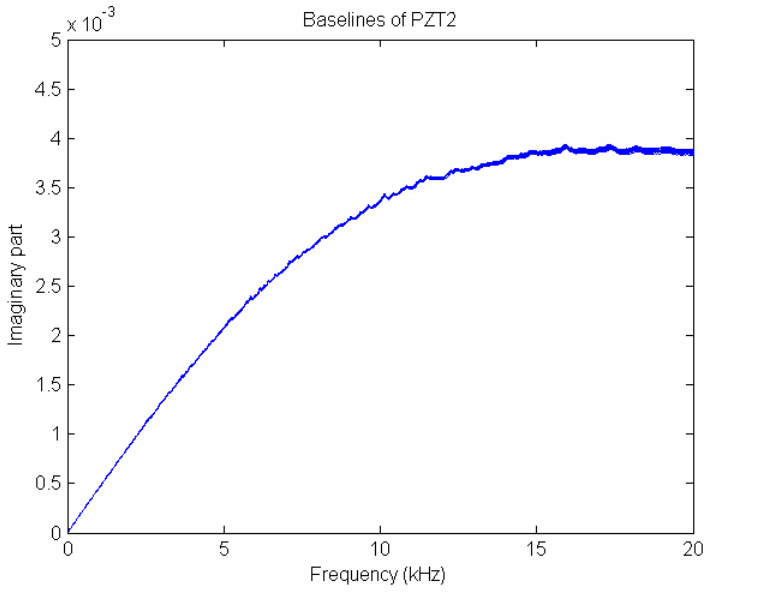


(b) PZT 2

**Figure 5:** Baseline Admittance Measurements from PZT patches. Total 14 measurements are shown.

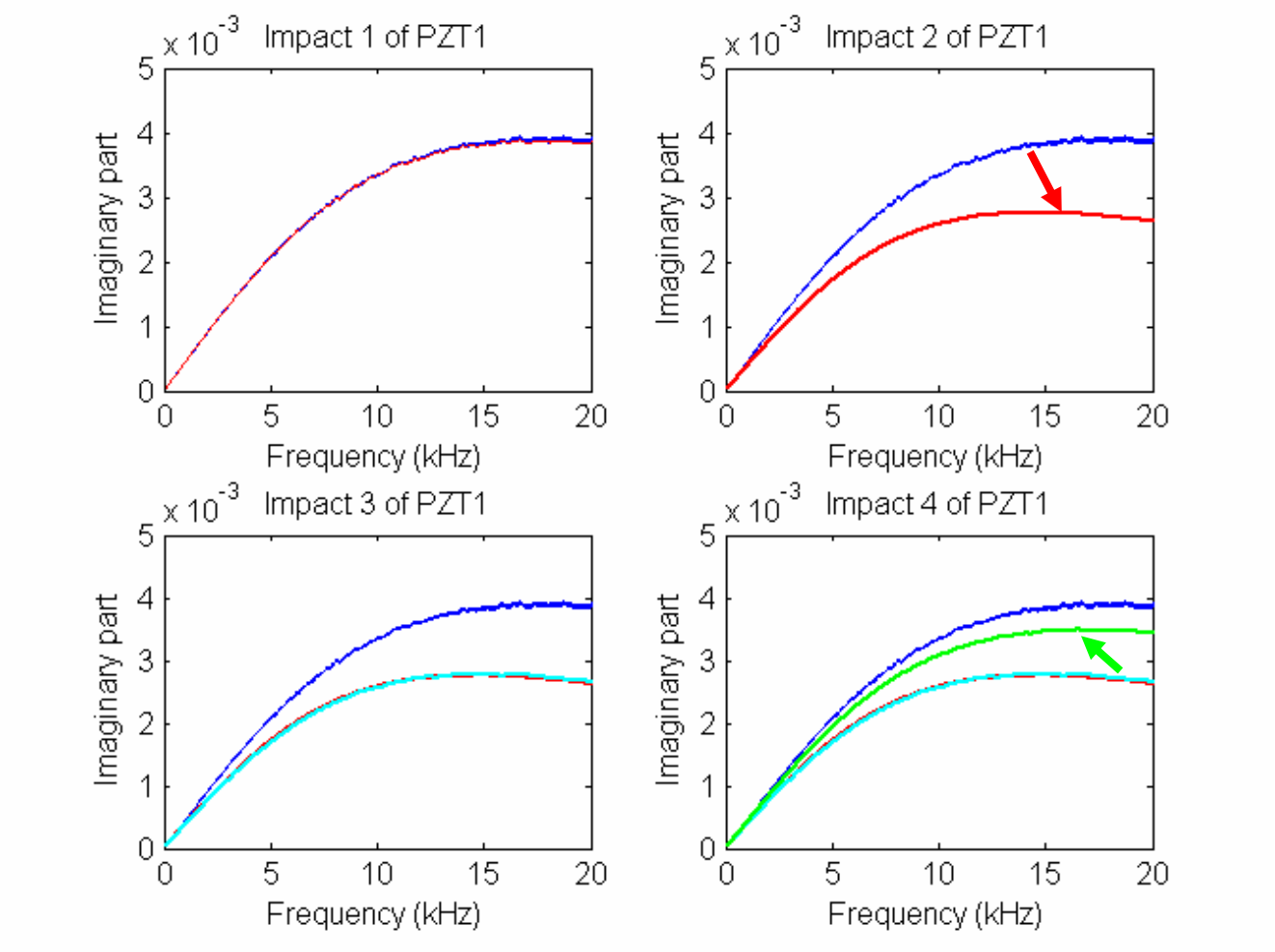


**Figure 6:** Baselines and Impact responses from PZT 1

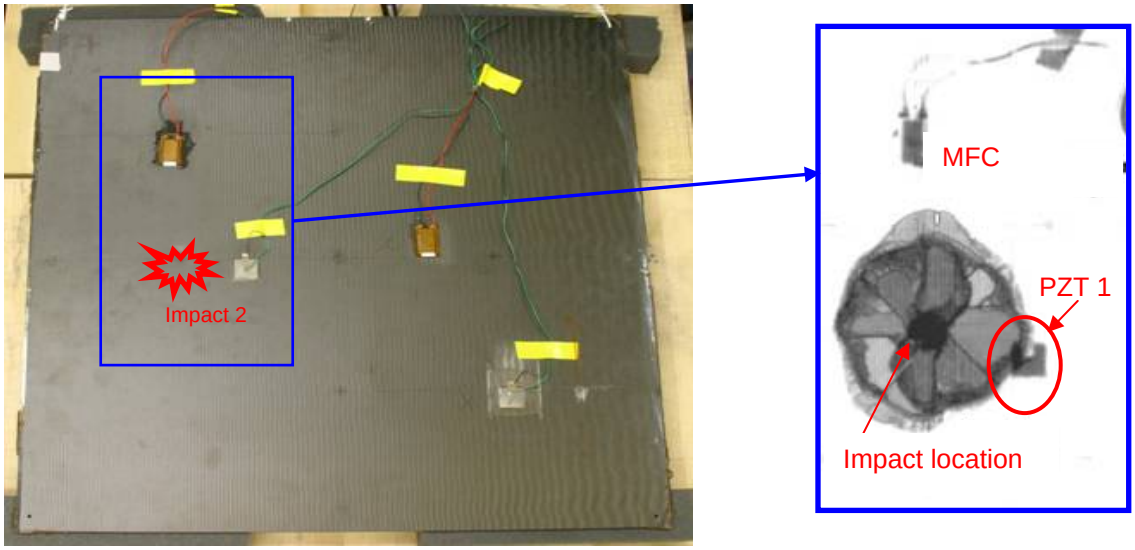


**Figure 7:** Delamination induced by Impact 2.

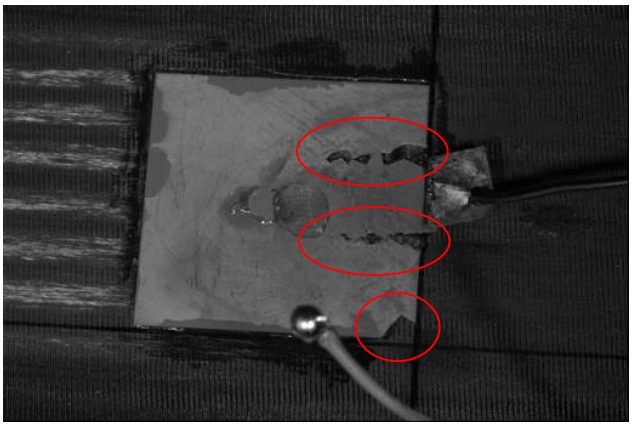

**Figure 8:** The failure of PZT sensor after Impact 5

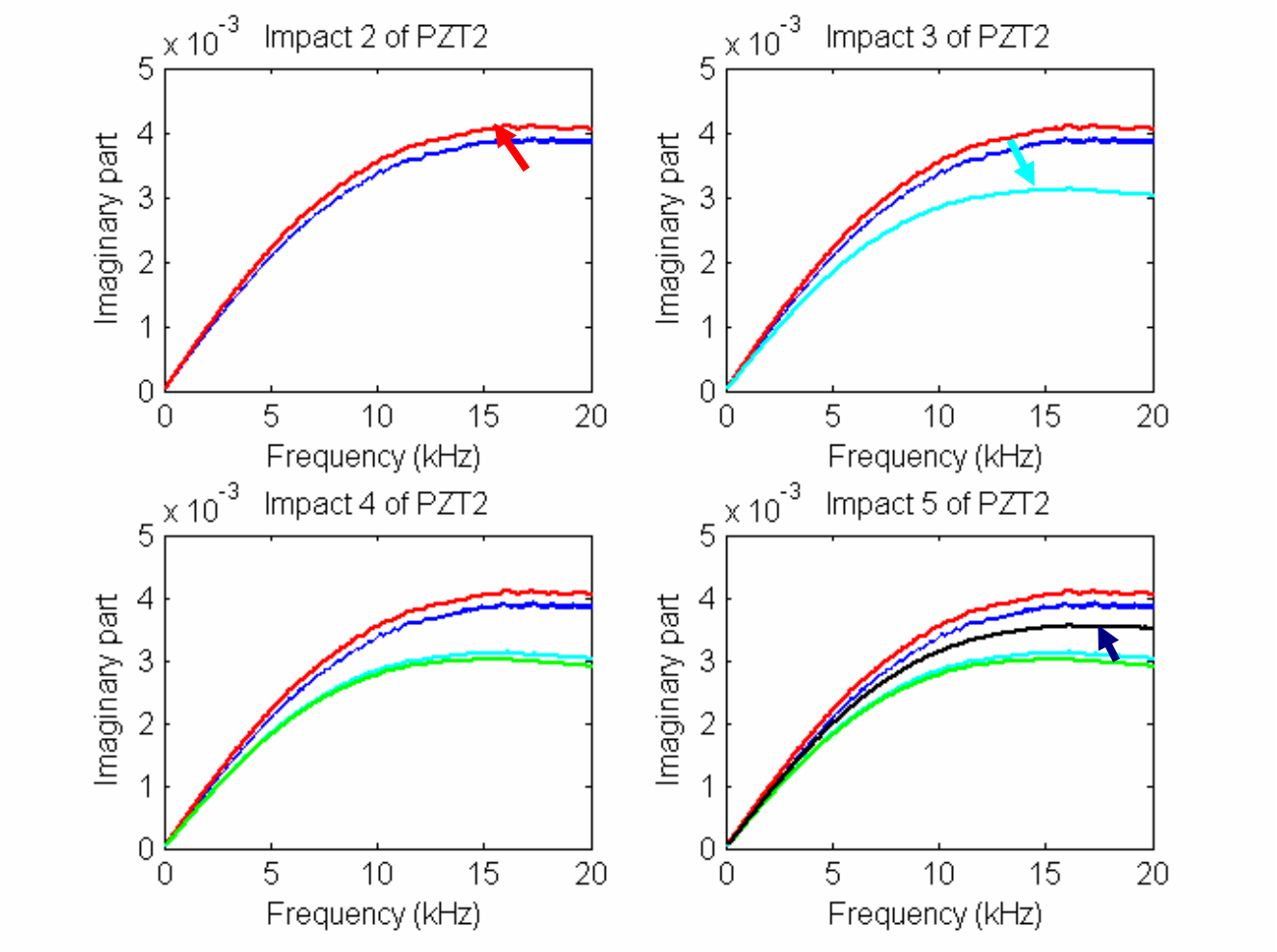


**Figure 9:** Baselines and Impact responses from PZT 2.

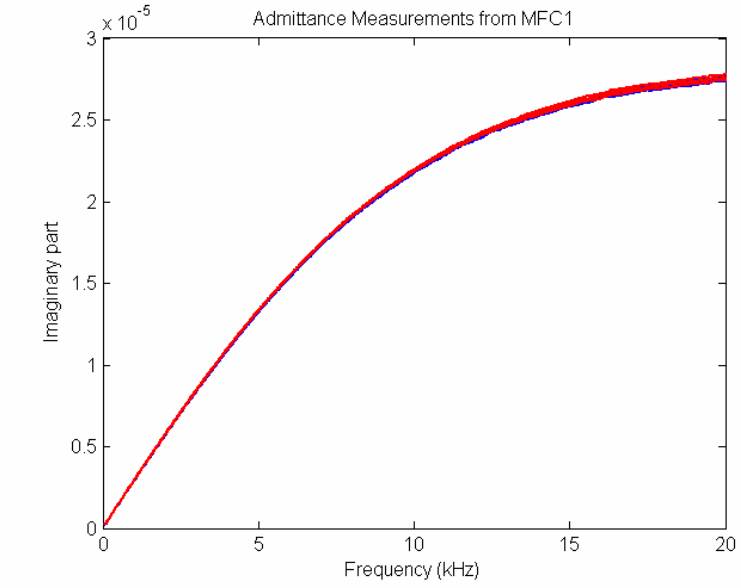


(a) MFC 1

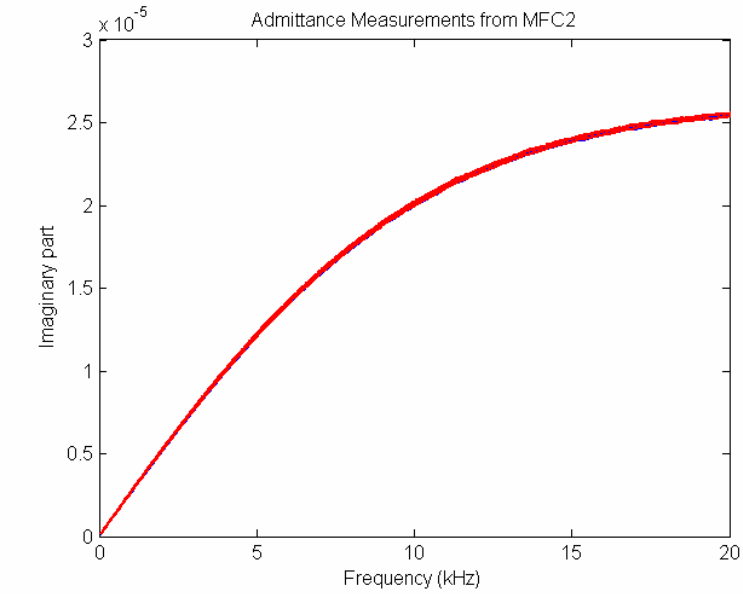


(b) MFC 2

**Figure 10:** Superposed baselines and impact responses from MFCs

| Tests | Impact Speed (m/s) | Location of Impact (mm) | |
|---|---|---|---|
| | | Distance from left edge | Distance from bottom edge |
| Impact 1 | 31.09 | 456.6 | 304.2 |
| Impact 2 | 39.93 | 152.4 | 304.2 |
| Impact 3 | 36.88 | 342.3 | 152.4 |
| Impact 4 | 35.66 | 266.7 | 456.6 |
| Impact 5 | 32.92 | 304.2 | 304.2 |

Table 1. The impact speeds and locations